



Ultrasonic properties of all-printed piezoelectric polymer transducers

Sanat Wagle, Adit Decharat, Peter Bodö, and Frank Melandsø

Citation: [Applied Physics Letters](#) **103**, 262902 (2013); doi: 10.1063/1.4857795

View online: <http://dx.doi.org/10.1063/1.4857795>

View Table of Contents: <http://scitation.aip.org/content/aip/journal/apl/103/26?ver=pdfcov>

Published by the [AIP Publishing](#)



FREE Multiphysics Simulation e-Magazine

DOWNLOAD TODAY >>

COMSOL

Ultrasonic properties of all-printed piezoelectric polymer transducers

Sanat Wagle,¹ Adit Decharat,¹ Peter Bodö,^{2,a)} and Frank Melandsø^{1,b)}

¹Department of Physics and Technology, University of Tromsø, 9037 Tromsø, Norway

²Acreo AB, Box 787, 60117 Norrköping, Sweden

(Received 20 September 2013; accepted 11 December 2013; published online 26 December 2013)

The ability of producing ultrasonic transducers from screen-printing has been explored experimentally, through printing and characterization of a large number of transducers. In an all-printed test design, 124 transducers with four different electrode sizes ranging from 1 to 4.9 mm², were printed layer-by-layer on a high performance polyethyleneimine polymer. Inks from ferroelectric and conductive polymers were applied to the active part of a transducer, to provide a good acoustical match between the individual layers. Ultrasonic characterizations of the transducers done by two independent methods provided a broad-banded frequency response with a maximum response around 100 MHz. © 2013 Author(s). All article content, except where otherwise noted, is licensed under a Creative Commons Attribution 3.0 Unported License. [<http://dx.doi.org/10.1063/1.4857795>]

Ferroelectric polyvinylidene fluoride (PVDF) and its copolymer PVDF trifluoroethylene [P(VDF-TrFE)] are widely used for making ultrasonic sensors and transducers applied to nondestructive evaluation (NDE), underwater acoustic and medical imaging.¹⁻⁹ Although piezoelectric polymers have a considerable weaker piezoelectrical coupling than comparable ceramics, they have advantages in terms of being flexible, easy to process, and providing a relatively good acoustic match to water, human tissue, and many polymer materials. A large number of techniques have been explored for processing ferroelectric polymers into flexible film, such as spin coating, hot pressing, stamping, and spraying.¹⁻⁷ Electrodes can also be attached to the film surface by various methods, as, for example, sputter coating, vapor deposition, and printing.^{4,6,9-14} Some of the printing methods (e.g., screen-printing, ink-jet printing, and laser ablation) also facilitate electrode printing directly onto the backing substrate, with a potential reduction in processing steps and fabrication time.⁹⁻¹⁴ It was recently shown that the P(VDF-TrFE) material can be screen-printed in the fluid phase and integrated with screen-printed electrodes as an all-printed touch sensor that utilizes the material's pyroelectrical property.¹⁴ The piezo- and pyro-electrical coefficients for screen-printed sensors were also found comparable to sensors made from conventional processing methods,¹⁴ and the suggested printing method is therefore very attractive with respect to cost reduction and processing time, especially for the large area sensor industries.

In this Letter, we have investigated the possibility of producing high frequency ultrasonic transducers as an all-printed device. The active part of this device uses a conductive polymer [poly-3,4-ethylene-dioxythiophene (PEDOT) doped with poly-styrenesulfonate (PSS)] as the electrode material, in a 3-layered printed structure of PEDOT:PSS-P(VDF-TrFE)-PEDOT:PSS. The PEDOT:PSS electrode material was chosen due to its suitability for screen-printing

and good acoustic impedance match to P(VDF-TrFE). The combination of PEDOT:PSS and P(VDF-TrFE) have previously been used in actuators,¹⁵ and loudspeakers.¹⁶ One should note that the conductivity of PEDOT:PSS is relative low compared to, e.g., inks containing metallic particles, and therefore limits the electrode size that can be used for a given frequency. For high frequency applications, it is also crucial to minimize the length of conductive lines supporting the electrodes if these are made from PEDOT:PSS or to overprint/extend these lines by materials with much higher conductivity. For our design, we chose to overprint and extend lines outside the active transducer area by a silver ink (Ag 5000 from DUPont) with an interfacing carbon ink (C7 102, DUPont). A PEDOT:PSS ink from Agfa (Orgacon EL-P5015) was chosen due to its high conductivity and good attachment to P(VDF-TrFE). To increase the conductivity further, each PEDOT:PSS layer was also printed two times with an intermediate curing cycle of 130 °C.

To test the proposed design and materials, several test sheets with approximately A4 size were printed by the Swedish company Acreo AB using a P(VDF-TrFE) ink similar to the one reported in Ref. 14 with a weight ratio 70:30 between VDF and TrFE. As the under laying printing substrate also acts as the transducer backing material, the high performance polymer Ultem 1000 was chosen with a sheet thickness of around $h=0.85$ mm. This substrate material made from polyethyleneimine (PEI) provides very good thermal stability (for our processing temperatures ≤ 130 °C), good impedance match to other printed materials, and a very low acoustic attenuation. The latter property in combination with the fairly thin substrate enable us to estimate important transducer properties (e.g., emitted acoustic amplitude and frequency response) from the acoustic reflection generated from the polymer-air interface at the backside of the substrate. Each of these A4 sheets contains 124 transducers with four different transducer layouts, where the shape of the active electrode area is varied. This includes one transducer with a rectangular 1.0 mm \times 1.0 mm electrode (which we hereafter will refer to as T1) and three transducers (referred to as T2, T3, and T4) with circular electrodes with diameters

^{a)}Present address: Svärtinge Udde 16, 60599 Norrköping, Sweden

^{b)}Author to whom correspondence should be addressed. Electronic mail: frank.melandso@uit.no.



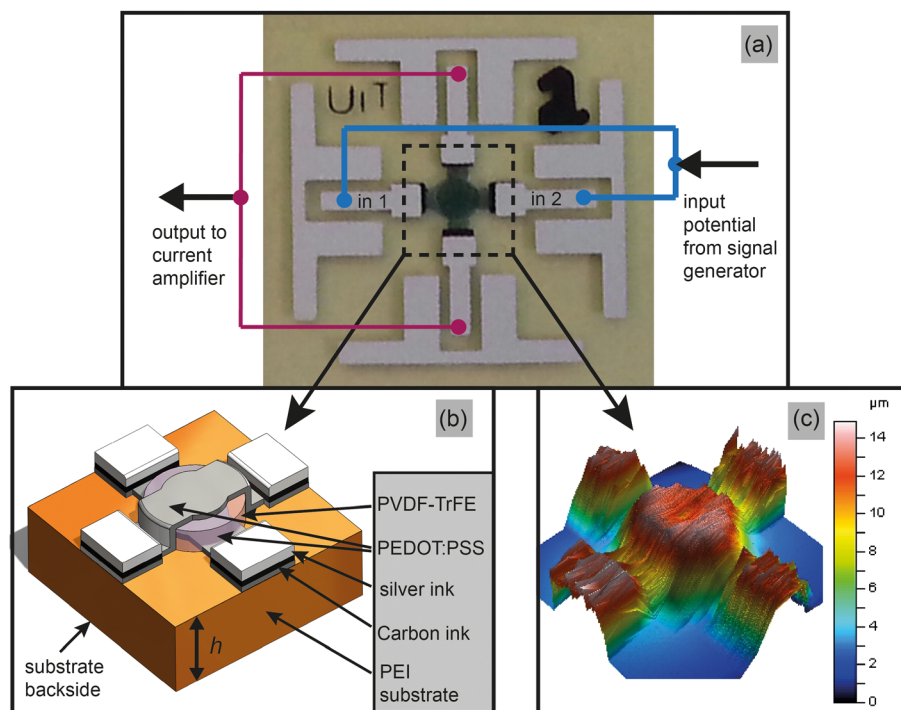


FIG. 1. Example of a screen printed transducer cell shown as an image [Fig. (a)] and as a 3-D illustration [Fig. (b)] showing the various layers in the central domain (inside the indicated rectangular). The height of this central region as measured by a surface profiler is shown in Fig. (c).

of $d = 1.5$ mm, 2.0 mm, and 2.5 mm, respectively. After the printing, the A4 sheets were cut into smaller transducer panels (with size 40 mm \times 40 mm) containing only four transducers to simplify further characterizations.

A transducer of type T3 (with a circular electrode with a diameter of $d = 2.0$ mm) is shown in Fig. 1, as a close-up image [Fig. 1(a)] and as a 3D drawing [Fig. 1(b)] identifying the location of different materials in the central region. The height of the printed layers in the central region was also measured using a KLA/Tencor P6 surface profiler [Fig. 1(c)]. From profiling a large number of transducers, the total thickness of the active transducer area was measured to be around 10 μm with an average rms surface roughness of 0.4 μm . The thickness of the lower PEDOT:PSS electrode was measured to 2.1 μm from a test printing located at a different position on the substrate, yielding a P(VDF-TrFE) thickness of 5.8 μm by assuming the same thickness as for the top electrode. Comparable thicknesses are also estimated from jumps in the transducer profiles, although the combined surface roughness and variations between samples impose some uncertainty.

In order to enhance the crystallinity of P(VDF-TrFE) and thereby its piezoelectric effect, the small transducer panels were annealed for approximately 40 min at 130 $^{\circ}\text{C}$ and then poled at room temperature by connecting a high frequency voltage source to the electrodes.^{2,17} They were poled by using an AC voltage with frequency of 0.25 Hz over 10 periods. A Sawyer-Tower circuit was used to monitor the poling of four typical transducers samples of type T1 to T4 (also used further in the ultrasonic characterization). After measuring the potential on the reference capacitor used in this circuit by a high-impedance multi-meter (Agilent 34411A 6 1/2), and compensating for a small constant leakage current, we obtain displacement field D versus applied electrical field E with well-known hysteresis loops as shown in Fig. 2. Here, it should be noticed that all four sensor types

show almost symmetrical hysteresis loops with saturation around 100 MV/m, giving a remanent polarization of about 70 mC/m² and a coercive field of about 50 MV/m, which are in good agreement with previous results reported for screen-printed¹⁴ and spin coated¹⁷ sensors. After removing the sensor from poling, it was kept for relaxation for at least 12 h to eliminate excess charge.

To characterize the acoustic response, each of the transducers in the panel were connected directly onto a PCB using small spring contacts in order to minimize additional inductive and capacities effects caused by open connectors. Two independent characterization instruments were then, in sequential order, connected to this PCB. The first instrument was an electrical impedance analyzer (TREWMAC System TE1000) applied in the frequency ranges from 20 MHz up to 150 MHz, which is the highest available frequency. The amplitude of the admittances (the inverse of the measured

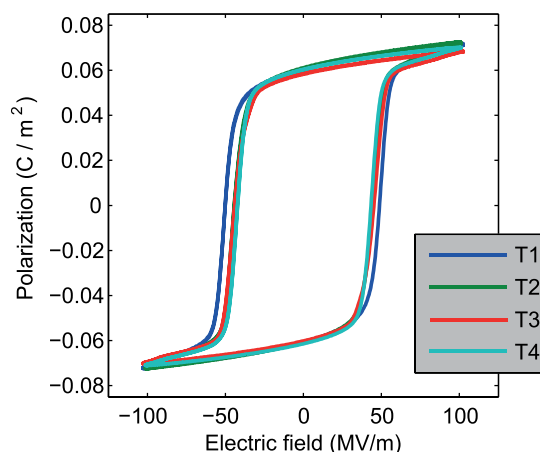


FIG. 2. Hysteresis loop for test samples T1 to T4 as measured from the Sawyer-Tower circuit.

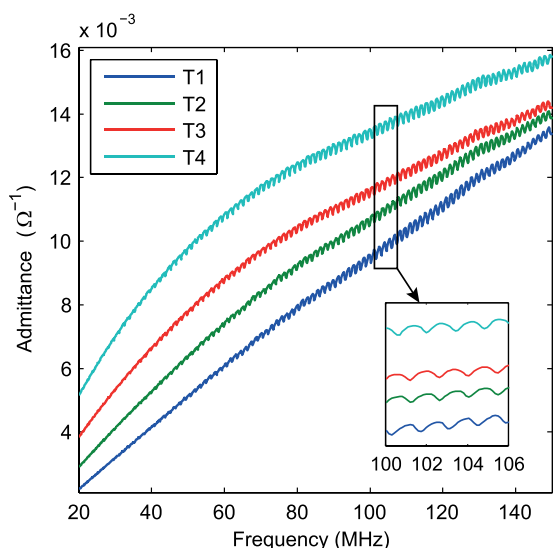


FIG. 3. Magnitude of admittance as measured from the impedance analyzer. The inset figure shows a magnified view of the indicated domain.

impedance amplitude) for the T1 to T4 transducer samples is shown in Fig. 3 together with a magnified inset figure for frequencies between 100 and 106 MHz. For all electrode sizes, we observe oscillations that are superimposed onto background levels that increase with frequency. These oscillations that cover most parts of the scanned frequency range are produced from standing wave features in the PEI substrate. We note that all samples generate almost similar oscillation periods of around $f_0 = 1.4$ MHz estimated from the inset figure. If we assume free boundary conditions (good approximation for the surrounding air) and neglect the thicknesses and masses induced by the printed layers, the fundamental frequency, which also determines the oscillation period, must satisfy $h = \lambda/2$, where λ is the wavelength and h is the substrate thickness. This yields a phase velocity estimate $v_0 = 2hf_0 \approx 2400$ m/s for $h = 0.85$ mm.

The second measurement setup consists of an arbitrary wave generator (Agilent 81150A) used to drive the transducers, and a current amplifier (FEMTO DHPKA-100) connected to the counter side electrode (see the connection points indicated in Fig. 1(a)). The output from this amplifier was then sampled by a digital oscilloscope (Yokogawa DLM

6054), which can digitize up to a 12 bit accuracy when operating in high resolution modulus. In order to generate wide band acoustical echoes from the backside of the PEI backing [see Fig. 1(b)], the signal generator was programmed to give the output potential

$$V(t) = V_0 \left[1 - \frac{(t - t_0)^2}{\sigma^2} \right] \exp \left[-\frac{(t - t_0)^2}{2\sigma^2} \right].$$

This potential that has the shape of the second derivative of a Gaussian with a characteristic width, σ , is normalized to give potential V_0 at the pulse firing time t_0 . For our case, the output of the signal generator was adjusted to provide 4.5 V peak to peak, which turned out to be sufficient for producing a good signal to noise ratio after averaging over 256 pulse shootings. The pulse width σ was adjusted to maximize the amplitudes of the received echoes, yielding $\sigma = 2.0$ ns.

Figure 4(a) shows the first reflection (FR) from the PEI backside as a function of time after firing ($t - t_0$) as it is digitized from the output of the current amplifier. One should note that for all samples T1 to T4, we have observed echoes from thickness extension waves (longitudinal modes) only. This is as expected due to the size of the active transducer areas, which for all samples, are much larger than the corresponding printing thicknesses.^{3,8} We also see a slight difference in echo receiving time for the four samples, which are mainly caused by variations in the substrate thicknesses (measured by a micrometer to 0.862 mm, 0.853 mm, 0.849 mm, and 0.859 mm for samples T1 to T4, respectively). An estimate based on the time difference between the first and the second echo then gives longitudinal velocities of 2450 m/s, 2460 m/s, 2460 m/s, and 2480 m/s for the respective samples, slightly larger than the phase velocity of 2400 m/s estimated from the impedance data. Our PEI velocity estimates also compare quite well to values reported in Ref. 18 for Ultem 1000, e.g., with a longitudinal wave velocity around 2420 m/s at 20 °C.

Figure 4(b) shows the frequency spectrum in a decibel (dB) scale for the measured driver pulse for T1 together with the dB spectra of the FR obtained by taking the local Fourier pulses in Fig. 4(a). The measured spectra for the pulses used to drive T2 to T4 are very similar that for T1, and are therefore not shown in the figure.

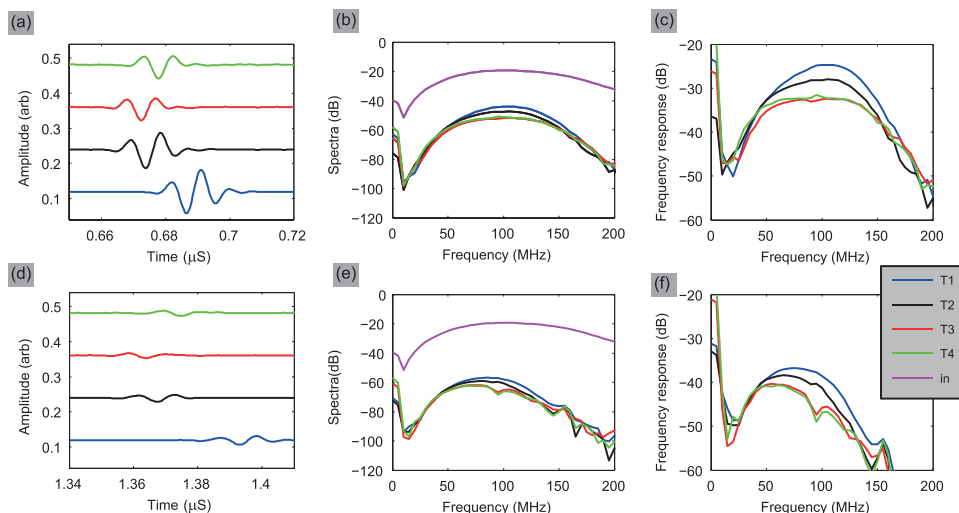


FIG. 4. Here, Fig. (a) shows the measured first reflection from the PEI air interface for the 4 samples where DC values have been added to visually separate the pulses. Figure (b) illustrates the corresponding output spectra in dB together with the measured spectrum of the driver pulse (upper curve). Figure (c) shows the difference between the output and input dB spectra, estimating the transducer’s frequency response. Figures (d)–(f) show the results corresponding to Figures (a)–(c) for the second reflection.

We have also estimated the frequency response for our samples from the ratio between the output and input spectra of the FR. This ratio in dB shown in Fig. 4(c) is obtained by subtracting the input spectrum from the corresponding output spectrum for the dB scale shown in Fig 4(b). From Fig. 4(c), it is easy to determine a central frequency f_c where the maximum response occurs, and -6 dB bandwidth for each sample, which are listed in Table I. One should be aware of several factors that may influence the measured acoustic responses, for example, the bandwidth of the used instruments (e.g., the current amplifier's 200 MHz bandwidth), and wave effects such as diffraction and attenuation. Since diffraction and attenuation both will reduce the energy for the waves scattered back for the backside of the substrate, both our characterization methods may, in fact, underestimate some of the spectral components as emitted from the transducer. To estimate the influence of these wave effects, we have repeated the calculations in the (a) to (c) figures for the second reflection, with results are shown in Figs. (d)–(f), respectively. A comparison between Figs. 4(c) and 4(f) will then give us the changes in spectral contains as the wave propagates through the substrate and back again. These figures suggest a significant wave damping through the substrate, e.g., around 12 dB at 100 MHz, which also estimates how much higher this spectral value will be at the transducer surface compared to what is shown in Fig. 4(c). The differences in the maximum response frequencies for Figs. 4(c) and 4(f) will also estimate the shift of f_c toward higher frequency at the transducer, e.g., around 20 MHz for T1 that is easiest to estimate.

It is interesting to compare the transducer data in Table I with other data reported for polymer transducers with comparable thicknesses, although the backing material and transmission medium might vary. For example, focused copolymer transducers on aluminum substrates have been reported in Refs. 1 and 2 both with a film thickness of around $6.0 \mu\text{m}$. These works reported central frequencies of 53 MHz and 40 MHz and -6 dB bandwidth of 83% and 83%, respectively. Moreover, a focused P(VDF-TrFE) copolymer transducers with $5.0 \mu\text{m}$ thick film on copper substrate³ showed central frequencies of 110 MHz in better agreement with our findings, and significantly higher than that obtained in Refs. 1 and 2. These high frequency transducers, which all use backing materials with acoustic impedances significant higher than the one for P(VDF-TrFE), yielded a theoretical maximum frequency around the $s = \lambda/4$ resonance, where s denotes the P(VDF-TrFE) thickness. This resonance will be around 100 MHz for $s = 6.0 \mu\text{m}$, assuming a P(VDF-TrFE) longitudinal velocity of 2400 m/s,⁸ or just slightly lower than the values listed in Table I. Our printed transducer layout has also been investigated as a finite element model (FEM) in the software

TABLE I. Measured transducer performance.

Trans. type	Central frequency f_c (MHz)	-6 dB band width (in MHz)	-6 dB band width (in % of f_c)
T1	108	71	65.74
T2	108	79	73.15
T3	101	92	91.10
T4	102	92	90.20

package COMSOL Multiphysics, which provided $f_c \sim 110$ MHz for cases where the PEI attenuation and electrode resistivity were neglected. We also used the FEM model to estimate the sheet resistance, by adjusting the conductivity in the numerical model until it fitted the resistivity that we measured between the input ports *in 1* and *in 2* shown in Fig. 1(a). We then obtained a mean PEDOT:PSS sheet resistivity $111.5 \Omega/\text{sq}$ with standard deviation $2 \Omega/\text{sq}$ for samples T1 to T4 using the measured PEDOT thickness $2.1 \mu\text{m}$ and neglecting the resistivity in the line segments covered by Ag and C inks. This estimate is within the sheet resistivity interval of 50 – $150 \Omega/\text{sq}$ specified by the PEDOT ink producer.

To summarize, we have shown that it is possible to produce all-printed ultrasonic transducers with PEDOT:PSS as the electrode material, yielding broad banded ultrasonic spectra with maximum frequency responses around 100 to 110 MHz. The shape of the estimated frequency response for these transducers as shown in Fig. 4(b), depend quite strongly on the electrode area, e.g., with a relatively flat response for the largest T3 and T4 samples. This behavior suggests that the conductivity of the printed materials is not sufficiently large to support these electrode sizes at the highest frequencies, and the transducer response therefore saturates at some cut-off frequency f_s significant lower than the transducer resonance frequency f_r (estimated from the FEM model to be around 110 MHz). This cut-off frequency will be determined by the transducer capacitance [through the electrode area and P(VDF-TrFE) thickness], and by the overall resistant loss, primarily through the PEDOT:PSS electrode itself and through the short PEDOT:PSS lines connecting the electrodes to the carbon and silver material [see Fig. 1]. It is therefore important to minimize the resistance in all areas using conductive polymers, e.g., by applying PEDOT:PSS with high conductivity and/or performing multiple screen-printings with this material.

We also observe that the transducer T1 with the smallest electrode area has a spectrum shape comparable to what we have seen before from other transducers with electrodes made from high conductive materials (e.g., sputtered gold). It is therefore likely that T1, which also yields the strongest acoustical response among the 4 samples [see Fig. 4(a)], has $f_s \geq f_r$. Our experimental findings therefore suggest that the PEDOT:PSS electrode area has to be of the order of 1 mm^2 or smaller, to fully take advantage of the broad bandwidth imposed by the thin printed P(VDF-TrFE) film.

This work was supported by The Research Council of Norway through the project “Subsea Sensors.”

¹C. H. Chung and Y. C. Lee, *NDT & E Int.* **43**, 96 (2010).

²M. Robert, G. Molingou, K. Snook, J. Cannata, and K. K. Shung, *J. Appl. Phys.* **96**, 252 (2004).

³K. Kimura and H. Ohigashi, *J. Appl. Phys.* **61**, 4749 (1987).

⁴L. F. Brown, R. L. Carlson, and J. M. Sempson, *Proceeding of the 1997 IEEE Ultrasonic Symposium* (IEEE, New York, 1997), p. 1725.

⁵T. Lillichorn, T. Blom, U. Simu, and S. Johansson, in *Proceedings of the 2005 IEEE Ultrasonic Symposium* (IEEE, Rotterdam, 2005), p. 1618.

⁶H. J. Kim, H. Lee, and B. Ziaie, *Biomed. Microdevices* **9**, 83 (2007).

⁷V. T. Rathod, D. R. Mahapatra, A. Jain, and A. Gayathri, *Sens. Actuators* **163**, 164 (2010).

⁸F. S. Foster, K. A. Harasiewicz, and M. D. Sherar, *IEEE Trans. Ultrason. Ferroelectr. Freq. Control* **47**, 1363 (2000).

- ⁹S. Karki, M. Kiiski, M. Myntysalo, and J. Lekkala, *Proceedings of the XIX IMEKO World Congress, Fundamental and Applied Metrology* (Lisbon, Portugal, 2009), p. 1765.
- ¹⁰S. Webster and T. D. Binnie, *Sens. Actuators, A* **49**, 61 (1995).
- ¹¹K. I. Arshak, D. McDonagh, and M. A. Durcan, *Sens. Actuators, A* **79**, 102 (2000).
- ¹²M. Dietze and M. E. Souni, *Sens. Actuators, A* **143**, 329 (2008).
- ¹³F. Bellan, A. Bulletti, L. Capineri, L. Masotti, G. G. Yaralioglu, F. L. Degertekin, B. T. Khuri-Yakub, F. Guasti, and E. Rosi, *Sens. Actuators A* **123–124**, 379 (2005).
- ¹⁴M. Zirkl, A. Sawatdee, U. Helbig, M. Krause, G. Scheipl, E. Kraker, P. A. Ersman, D. Nilsson, D. Platt, P. Bodo, S. Bauer, G. Domann, and B. Statlober, *Adv. Mater.* **23**(18), 2069 (2011).
- ¹⁵C. S. Lee, J. Joo, S. Han, and S. K. Koh, *Sens. Actuators, A* **121**, 373 (2005).
- ¹⁶A. C. Hubler, M. Bellmann, G. C. Schmidt, S. Zimmermann, A. Gerlach, and C. Haentjes, *Org. Electron.* **13**, 2290 (2012).
- ¹⁷R. C. Naber, P. W. M. Blom, A. W. Marsman, and D. M. Leeuw, *Appl. Phys. Lett.* **85**, 2032 (2004).
- ¹⁸M. Fukuhara, *J. Appl. Polym. Sci.* **90**, 759 (2003).